## PAPER

# Phase transformation of $TiO_2$ nanoparticles by femtosecond laser ablation in aqueous solutions and deposition on conductive substrates†

Paola Russo,[a,b,c] Robert Liang,[a,b,c] Rui Xiu He[a,b,c] and Y. Norman Zhou ⬡ *[a,b,c]

Titanium dioxide ($TiO_2$) is a wide bandgap semiconductor that is chemically stable, non-toxic, and economical compared to other semiconductors and has been implemented in a wide range of applications such as photocatalysis, photovoltaics, and memristors. In this work we studied the femtosecond laser ablation of titanium dioxide powders (P25) dispersed either in water or deposited onto a fluoride-doped tin oxide (FTO) substrate. The process was used as a route to induce the phase-transformation of $TiO_2$ nanoparticles which was governed by laser parameters such as ablation time and power. It was observed that upon increase of the ablation time of $TiO_2$ dispersion in water a bandgap widening occurred, leading to the possibility of bandgap engineering of $TiO_2$ using controlled laser parameter profiles.

## 1. Introduction

Pulsed laser ablation in liquids (PLAL) is a powerful technique for the synthesis of different nanostructures in the colloidal state depending on the target employed.[1–4] This technique has been widely employed in the ablation of titanium targets for the synthesis of $TiO_2$ nanomaterials with different shapes, sizes and phases[5–11] depending on the laser parameters employed such as the laser wavelength,[8,12,13] laser pulse energy[9,11,14,15] and the type of liquid medium employed.[6,8,16,17] Titanium dioxide has been extensively researched for its photocatalytic properties and applications. In 1972, Fujishima reported the splitting of water under illumination using a rutile $TiO_2$ photoanode and a Pt counter electrode.[18] Since then, due to its chemical stability, low cost, and non-toxicity, $TiO_2$ has been used in a wide range of applications such as removing conventional and emerging organic contaminants in water,[19,20] photocatalytic[21–26] processes, sensor devices,[27,28] and solar cells.[29,30] In nature, $TiO_2$ occurs in three crystalline polymorphs: rutile, anatase and brookite. $TiO_2$ is an n-type semiconductor and the three polymorphs possess different bandgap energies due to the differences in lattice structures.[31]

Specifically, rutile has a bandgap of 3.0 eV, while anatase and brookite have bandgaps of 3.2 eV and 2.96 eV, respectively.[32] Anatase is often used as a photocatalyst, rather than rutile, due to its greater photocatalytic activity.[31] However, several studies have shown that a mixture of anatase and rutile has greater photocatalytic activity than pure anatase.[33–35] Generally, the most employed formulation of $TiO_2$ is P25 Aeroxide™ made of 70–75% of anatase and 30–25% of rutile, where the enhanced activity arises from the increased efficiency of electron–hole separation due to the heterojunctions formed between anatase and rutile particles.[31] The interfacial charge carrier transport in $TiO_2$ anatase–rutile heterojunctions occurs in two pathways. One pathway is that the anatase phase will donate an electron to rutile due to its lower conduction band (CB) minimum. Another pathway is that the electrons will move from rutile to anatase *via* lower energy trapping sites in the anatase phase.

Under ambient conditions, rutile is the most stable crystal phase in bulk, while the other two polymorphs are considered as metastable phases, and upon heating an irreversible phase transformation into rutile occurs.[36] Several studies demonstrated that the particle sizes play a key role in the determination of phase stability.[31,37] For particle sizes less than 11 nm, anatase will be the most thermodynamically stable phase, while for dimensions between 11 and 35 nm, brookite is the most stable phase. When the sizes are greater than 35 nm, rutile is the most stable phase.[31] Anatase nanoparticles may be obtained using several processes, which include sol–gel,[38] hydrothermal[39] and solvothermal[40] methods. Heat treatment of these nanoparticles will produce rutile nanoparticles at a specific phase transformation temperature.

*[a]Waterloo Institute for Nanotechnology, University of Waterloo, 200 University Ave., West Waterloo, Ontario N2L 3G1, Canada. E-mail: nzhou@uwaterloo.ca*
*[b]Centre for Advanced Materials Joining, University of Waterloo, 200 University Ave., West Waterloo, Ontario N2L 3G1, Canada*
*[c]Department of Mechanical and Mechatronics Engineering, University of Waterloo, 200 University Ave., West Waterloo, Ontario N2L 3G1, Canada*
†Electronic supplementary information (ESI) available. See DOI: 10.1039/c7nr00201g

The possibility to control the conditions that affect the phase transformation is important. The phase stability of titania has a key role in the design of electronic devices because the properties and the performance of these materials may be affected[32,41] by the alteration of the crystalline phase.[41,42] It is commonly believed that the reason for the phase transformation from anatase to rutile should be attributed to the increase in the particle size induced by the sintering process that takes place at elevated temparatures.[37] However, more studies should be performed in order to better understand the physical and chemical processes involved in the phase transformation, as well as the mechanisms to promote or inhibit it.[43–46]

In this work we studied the phase-transformation of a dispersion of $TiO_2$ (P25, Aeroxide™) induced by femtosecond laser ablation under two conditions: (i) in aqueous solution and (ii) when deposited on a fluoride-doped tin oxide (FTO) substrate. To the best of our knowledge, few studies have been performed on the effects of the femtosecond laser ablation of a dispersion of $TiO_2$ in water. For instance, in a recent report, the ablation of rutile powder in water with a femtosecond laser[47] was studied, which led to the formation of rutile, anatase and brookite nanoparticles.[47] The laser ablation of $TiO_2$ powders with a YAG:Nd$^{3+}$ solid state laser has also been reported,[48] where the powders were deposited onto a glass substrate and then laser ablated in air. In the work presented here, we report on the phase-transformation of $TiO_2$ nanoparticles by femtosecond ablation of $TiO_2$ (P25) either as a suspension or by electrophoretic deposition on FTO glass. The results of the experiments showed that the laser ablation process of the P25 suspension in water induces phase transformation from anatase to rutile and back again to anatase increasing the ablation time. Moreover, the bandgap of the material can be controlled, leading to the possibility of employing PLA of $TiO_2$ for bandgap engineering. Ablation of the deposited P25 on FTO resulted in transformation from the anatase to the rutile phase of the patterned area, making this technique suitable for laser patterning. Rutile, a higher refractive crystal phase, can scatter light more efficiently than anatase, and this opens the possibility of using these patterned substrates in various applications such as silicon solar cells, energy-harvesting devices, and dye-sensitized solar cells (DSSC).[49,50]

## 2.   Experimental

### 2.1.   Laser ablation of $TiO_2$ in water

A schematic of the setup employed for the laser ablation experiments is shown in Fig. 1. In our experiments 10 mg of P25 powder (Aeroxide™) was suspended in 10 ml of water and stirred with a magnetic stirrer for the entire duration of the experiments. Femtosecond laser ablation experiments were conducted using a Ti–sapphire laser (Coherent, Inc.) with a wavelength of 800 nm, repetition rate of 1 kHz, and pulse duration of 35 fs with the Gaussian beam distribution. The laser
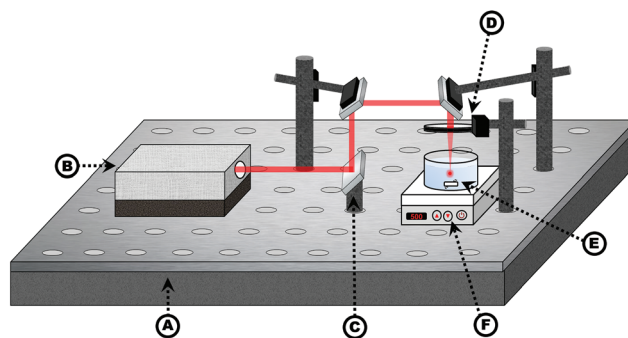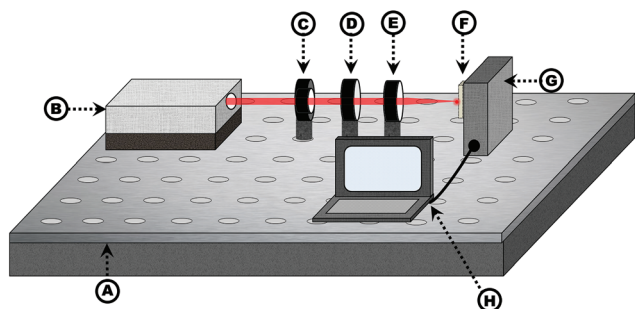


Fig. 1   Schematic of the femtosecond laser ablation experiment setup consisting of the (A) optical table, (B) Ti–sapphire laser, (C) mirror system, (D) focusing lens, (E) container containing a stir bar and $TiO_2$ solution, and (F) stirring plate.

ablation experiments were performed from the top in order to avoid laser reflections through the glass walls. The laser beam (80 μm in diameter) was focused inside the $TiO_2$ dispersion at 5 mm from the dispersion–air interface. The experiments were carried out at a power of 1.3 W (25.8 J cm$^{-2}$) and at different laser ablation times, in order to study the laser effects on the $TiO_2$ crystal structure as a function of ablation time. The P25 dispersions were ablated for 5, 15, 30, 60, 90 and 120 minutes and then the resulting ablated suspensions were characterized. Scanning electron microscopy (SEM) images of the dispersion deposited onto the silicon substrate were taken using a Zeiss Leo 1550 FE-SEM at an accelerating voltage of 10 kV. The crystal phase and structure of the ablated material were investigated by Raman spectroscopy and transmission electron microscopy (TEM). Raman spectra were measured using a Renishaw micro-Raman spectrometer with a He/Ne laser at an excitation wavelength of 632.8 nm. HRTEM observation was made using a JEOL 2010F at the Canadian Centre for Electron Microscopy (Hamilton, Ontario, Canada). The TEM samples were prepared by drop casting the dispersions onto lacey carbon grids. Ultraviolet-visible (UV-VIS) analysis of the laser ablated dispersions was carried out with a Shimadzu UV-2100 PC spectrophotometer over a spectral range of 190–600 nm.

### 2.2.   Deposition of $TiO_2$ onto FTO substrates (P25/FTO)

$TiO_2$ films were fabricated by electrophoretic deposition of P25 on fluoride-doped tin oxide (FTO) glass, followed by annealing. The $TiO_2$ dispersion was made by dispersing 1 g of P25 nanoparticles in 250 mL ethanol, 15 mL acetylacetone, 4 mL acetone, 2 mL water, and 27 mg iodine.[51] The dispersion was sonicated for 30 min and stirred for 1 hour. FTO glass (MTI Corp, 1″ × 3″ × 2.2 mm, TEC 7, $R$: 12–14 ohm sq$^{-1}$) was used as a support and cathode for $TiO_2$ deposition, while a titanium sheet was used as the anode. The cathode and anode were connected to a DC voltage supply and immersed in the aforementioned $TiO_2$ dispersion. The electrophoretic deposition onto 1″ × 1″ FTO glass was conducted at a constant voltage of 30 V for 60 seconds. The P25 deposited FTO substrate was dried in air and then heat-treated at 450 °C to improve adhesion.

**Fig. 2** Schematic of the femtosecond laser ablation setup for laser patterning consisting of the (A) optical table, (B) Ti–sapphire laser, (C) mechanical shutter, (D) neutral density filter, (E) focusing lens, (F) patterned substrate, (G) motorized stage, and (H) computer.

### 2.3. Laser patterning of $TiO_2$ on the FTO substrate

The patterning of P25 deposited on the FTO substrate was performed using the Ti–sapphire laser system described in section 2.1 and the setup was configured to pattern the substrate on a motorized stage controlled *via* a computer; the experimental setup schematic used is shown in Fig. 2. The sample was placed on a 2 axis stepper motor stage and a 5 cm line was patterned focusing the laser (80 μm in diameter) on the substrate at a speed of 1.5 mm s$^{-1}$. In total, 8 lines were patterned at increasing laser powers.

## 3. Results and discussion

### 3.1. $TiO_2$ phase transformation upon laser ablation in water

The laser ablation study of the $TiO_2$ nanoparticles was conducted by increasing the ablation time. After 15 minutes of irradiation the colour of the dispersions changed from white (as-purchased P25 Aeroxide™) to blue. The colour change can be attributed to the formation of $Ti^{3+}$ species that will lead to the formation of rutile $TiO_2$ nanoparticles.[6,47] The mechanisms underlying the formation of $TiO_2$ nanoparticles upon laser ablation of a Ti target have been widely discussed. The mechanism may be summarized in three steps, in which (1) the high temperature and pressure generated by the laser–matter interaction will produce a plasma plume; (2) the plasma plume undergoes ultrasonic adiabatic expansion, which causes rapid cooling of the plume and formation of titanium clusters; and (3) the titanium ions and clusters react with water molecules at the interfacial region between plasma and liquid, leading to the formation of rutile nanoparticles.[6,8,52]

Increasing the ablation time to 120 min led to dispersions that were less blue in intensity. In order to investigate whether a structural modification of the P25 nanoparticles was occurring during the laser ablation, the ablated dispersions were investigated using Raman spectroscopy, which is widely used for the characterization of $TiO_2$ polymorphs since it allows one to distinguish between the different phases of $TiO_2$.[53–55] The most prominent Raman features of anatase are the peaks centered at 144 cm$^{-1}$ ($E_g$), 197 cm$^{-1}$ ($E_g$), 399 cm$^{-1}$ ($B_{1g}$), 513 cm$^{-1}$

($A_{1g}$), 519 cm$^{-1}$ ($B_{1g}$), and 639 cm$^{-1}$ ($E_g$), while the Raman active modes of the rutile phase are at 143 cm$^{-1}$ ($B_{1g}$), 447 cm$^{-1}$ ($E_g$), 612 cm$^{-1}$ ($A_{1g}$) and 826 cm$^{-1}$ ($B_{2g}$).[56] The Raman spectrum of P25 possesses peaks containing the anatase and rutile phases, since it is made of 70–75% of anatase and 30–25% of rutile phases. The main peaks are centered at 636 cm$^{-1}$ ($E_g$), 515 cm$^{-1}$ ($B_{1g}$), 443.17 cm$^{-1}$ ($E_g$), and 394.52 cm$^{-1}$ ($B_{1g}$). In this work, Raman analysis was performed after depositing the laser treated dispersions onto glass slides and allowing them to dry in air under ambient conditions. The acquired spectra are shown in Fig. 3 and are compared to commercial anatase, rutile and P25 powders.

The laser-treated samples are compared to the as-received P25 in aqueous solution. After 5 minutes of laser treatment of dispersed P25, the peak centered at 636.4 cm$^{-1}$ blue-shifted by 1.59 cm$^{-1}$. From the comparison of the Raman spectra, structural modification of P25 started to take place after 15 minutes of laser ablation, as depicted from the spectrum (purple line), which depicts peak shifting as shown in Fig. 3. In particular, a blue-shift of 11.11 cm$^{-1}$ of the Raman mode at 636.4 cm$^{-1}$ was detected along with the peak broadening. Additionally, the intensity of the peak at 515.06 cm$^{-1}$ decreased, while the intensity of the peak at 443.17 cm$^{-1}$ increased and blue-shifted by 2.65 cm$^{-1}$. The peak at 394.52 cm$^{-1}$ red-shifted by 8.73 cm$^{-1}$ and the intensity of the peak decreased. The two peaks at 394.52 cm$^{-1}$ and 443.17 cm$^{-1}$ are relative to the Raman active modes ($B_{1g}$) and ($E_g$) of anatase and rutile phases, respectively, and are noteworthy. After 15 minutes of laser treatment, these two peaks give rise to a unique peak and the spectrum results are found to be similar to the Raman spectrum of rutile, suggesting a phase transformation from mainly anatase to mainly rutile nanoparticles. This evidence is further supported if we take into consideration the earlier observation of the color change of the dispersion to blue, which is attributed to the formation of rutile nanoparticles.[6,47] This result is in agreement with the mechanisms occurring
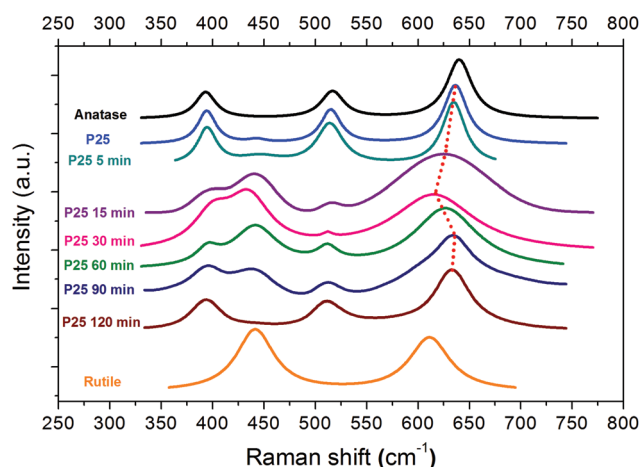


**Fig. 3** Raman spectra of P25 dispersions after 5, 15, 30, 60, and 120 minutes of laser ablation. For comparison, Raman spectra of anatase, rutile and P25 as purchased powders have been included.

during the laser ablation of titanium dioxide discussed earlier, which cause the formation of a plume containing titanium ions which upon expansion and successive cooling will form titanium clusters leading to the formation of rutile nanoparticles. The phase transformation to rutile is more apparent after 30 minutes of laser ablation, in which a peak shift to 614.98 cm$^{-1}$ occurs, which is within the reported value for rutile (611 cm$^{-1}$). Furthermore, the intensity of the peak at 511 cm$^{-1}$ decreases and the separation between the two peaks at 394.52 cm$^{-1}$ and 443.17 cm$^{-1}$ is reduced compared to P25 treated for 15 minutes. When the laser ablation was performed for 60 minutes, a redshift of 11.9 cm$^{-1}$ occurred and the peak center was found at 626.88 cm$^{-1}$, the intensity of the peak at 511.89 cm$^{-1}$ increased, and the separation between the two peaks at 397.7 cm$^{-1}$ and 441.31 cm$^{-1}$ was more evident. This suggests that the TiO$_2$ nanoparticles are of mixed phase composition containing rutile and anatase. It should be noted that the existence of a mixed phase upon laser ablation of the Ti target has been already reported by Tian *et al.* and it is a consequence of the rapid change of temperature and pressure during ablation.[57] The increasing of the laser ablation time up to 90 minutes causes either a decrease of the intensity of the band of the rutile phase at 437 cm$^{-1}$, or an increase of the band intensity relative to the anatase phase at 394.52 cm$^{-1}$. This indicates that the predominant phase of the nanoparticles is the anatase one. After 120 minutes of laser ablation there occurred a clear phase transformation into anatase. In the literature, the ratio of the integrated Raman peak intensity of the peak of rutile at 447 cm$^{-1}$ to that of anatase at 399 cm$^{-1}$ is used for the measurement of the weight ratio of rutile to anatase.[58,59] Fig. 4 depicts the integrated Raman peak intensity

ratio as a function of laser ablation time in order to visualize the anatase-to-rutile and rutile-to-anatase conversion as a function of laser ablation time. The commercial P25 and the nanoparticles ablated for 5 minutes showed a $I_{446}/I_{396}$ ratio of 0.2 indicating the presence of mostly crystalline anatase, which is in agreement with the recorded Raman spectra and with the $I_{446}/I_{396}$ value reported in the literature.[59] Increasing the ablation time causes an increase of the $I_{446}/I_{396}$ ratio to 1.1 which can be related to the formation of rutile nanoparticles. After 60 minutes of laser ablation the $I_{446}/I_{396}$ ratio reaches 1.8 indicating that the nanoparticles produced were predominantly rutile, which has already been demonstrated by the Raman spectrum analysis. The increase of the ablation time up to two hours introduced a phase transformation from rutile to anatase and this can be seen as a decrease in the $I_{446}/I_{396}$ ratio to 0.8 after 90 minutes and to 0.2 after 120 min, which is the value recorded for the un-treated P25, where anatase is the predominant phase. The trend shown in Fig. 4 is in agreement with the information obtained from the Raman spectrum analysis, in which one hour of laser ablation of P25 nanoparticles induces the formation of rutile nanoparticles; however, for prolonged ablation times a phase transformation to anatase takes place.

As previously described, the laser ablation in water causes the melting of the material and the generation of a plasma plume, which contains atoms, molecules, electrons, ions, and expands into the surrounding liquid, cools down and finally leads to the formation of the nanoparticles. It was reported from Koshizaki *et al.* that spherical nanoparticles are obtained when laser ablation is performed in a liquid environment.[60] The phase transformation from rutile to anatase is thermodynamically irreversible, however when the sizes of the particles decrease the phase stability reverses.[31] This is corroborated by studies that have reported about the size reduction of nanoparticles upon laser irradiation of nanoparticles using an unfocused laser beam.[60,61] On the basis of the current literature and the experimental results, we hypothesize that upon laser ablation of P25 aqueous suspension with a focused laser, two events might occur which lead to the phase transformation from rutile to anatase nanoparticles. The first process involves the generation of spherical particles from a localized volume that is ablated from the as-received P25 nanoparticles that appear square-like. Only the TiO$_2$ nanoparticles that cross the focus will melt and upon cooling spherical particles start to form. The formation of spherical particles is shown in Fig. 5(a–g), which represents the nanoparticles obtained at different ablation times. The second process that occurs is a decrease in the size of spherical nanoparticles with laser ablation time. As previously stated, a decrease in size of the nanoparticles could reverse the phase stability and this could be the reason for the transformation of rutile nanoparticles to anatase nanoparticles. The mechanism underlying the decrease in size could be explained if we consider that during the laser ablation not all the particles dispersed in the solution will cross the laser focus, consequently most of them will be
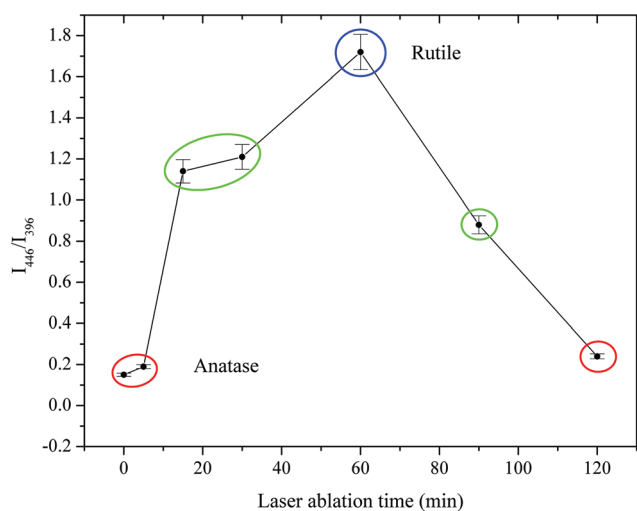


**Fig. 4** Integrated Raman peak intensity ratio as a function of laser ablation time for P25 dispersion. After 5 minutes of laser ablation the nanoparticles are in the anatase form (red circle), while after 20 minutes the transformation to rutile starts to occur (green circle). After 60 minutes of laser ablation the particles transformed to rutile (blue circle), however, upon increasing the ablation time (90 min), the particles start to transform to anatase (green circle) and after 120 minutes the particles possess the anatase phase (red circle).
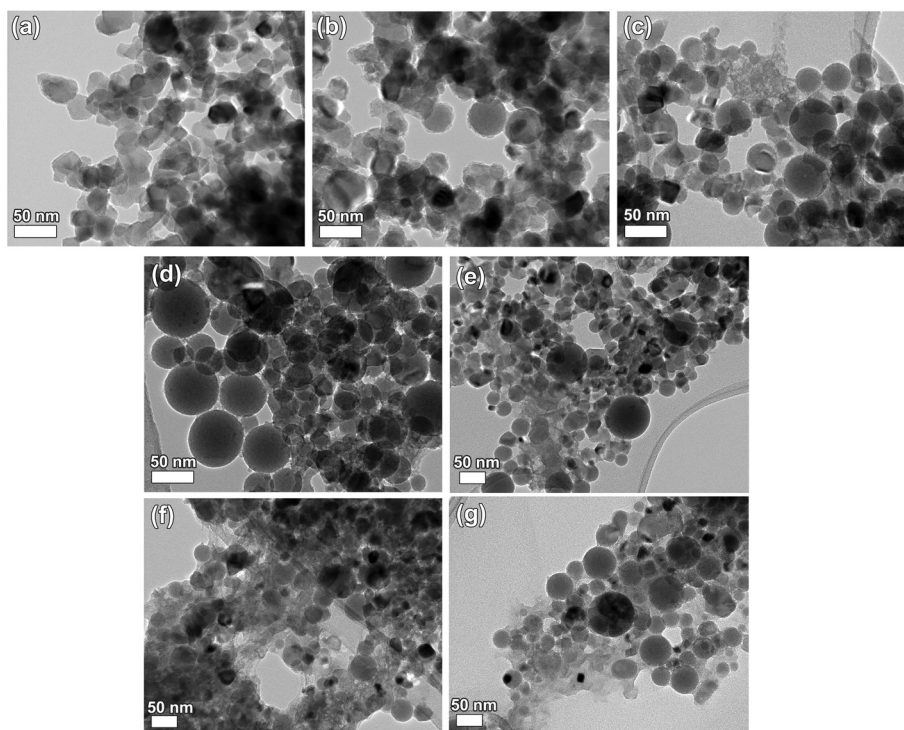
**Fig. 5** TEM images of P25 powders before (a) and after 5 (b), 15 (c), 30 (d), 60 (e), 90 (f) and 120 (g) minutes of laser ablation.

irradiated by the laser causing size reduction.[62–64] The decrease of the nanoparticle size can be attributed to fragmentation[52] that occurs during the laser treatment. Alnassar *et al.* reported about the decrease of size as a function of the pulse energy,[52] but it is also time-dependent.[63]

We observed that, after 15 and 30 minutes of PLA, there are more particles that have a size above 30 nm and it has been reported that when $TiO_2$ particles are bigger than 35 nm, the rutile phase is thermodynamically more stable than the anatase phase. In Fig. 6, HRTEM images of the samples at different ablation times are shown and from the analysis of the *d*-spacing (see Fig. S2A and S2B in the ESI†), it was confirmed that after 15 and 30 minutes of laser ablation, the particles were mainly rutile with a *d*-spacing of 0.32 nm along the (110) plane, as shown in Fig. 6(c and d) respectively. This result is in accordance with the Raman analysis which showed an increase of the rutile phase after 30 minutes of laser processing. Increasing the ablation time to 60 minutes led to the formation of particles with diameters over 35 nm, however smaller particles with diameters in the range of 9–20 nm are abundant.

These particles are in the anatase form with a d spacing of 0.35 nm along the (101) plane, as observed from the HRTEM image shown in Fig. 6(f), however rutile nanoparticles are also present (Fig. 6(e)). The coexistence of the small anatase particles and the bigger rutile ones can be explained on the basis of the two events that we hypothesized as occurring during the laser ablation process. The first event leads to the formation of the rutile nanoparticles with diameters of 35 nm, while the

irradiation causes the size decreasing and reversing of the phase stability, leading to a broadening of the size distribution. After 90 and 120 minutes of laser ablation the nanoparticles formed have similar dimensions to the nanoparticles obtained after one hour of laser ablation, but there is evidence that anatase nanoparticles have been produced, as seen from the HRTEM image shown in Fig. 6(h) and confirmed by Raman spectroscopy. From these results, it is evident that the laser ablation of P25 induced the formation of rutile particles mixed with smaller anatase nanoparticles. The size distribution analysis was conducted on the HRTEM images for laser ablated samples from 0 min to 120 min (Fig. S1†). One-way ANOVA statistics were conducted on P25 samples (Table S1†). All laser ablated P25 samples showed a significant increase in diameter ($p < 0.01$) compared to the untreated P25 sample. In general, increasing the irradiation time did not increase the diameter significantly. However, when the irradiation time was increased to 120 min, the diameter was higher than P25 samples irradiated at 5 min ($p = 0.003$) and 90 min ($p = 0.0121$).

In order to confirm the polymorphism and crystallinity of the laser treated P25 dispersions, we performed the XRD analysis of the samples before and after 5 and 60 minutes of laser ablation. The results are displayed in Fig. 7.

After laser treatment the dispersions showed the presence of both phases (anatase and rutile), as demonstrated by Raman spectroscopy and HRTEM analysis. The degree of crystallinity was calculated using the ratio of the intensity ($I_A/I_R$) of the strongest anatase reflection to the strongest rutile reflec-
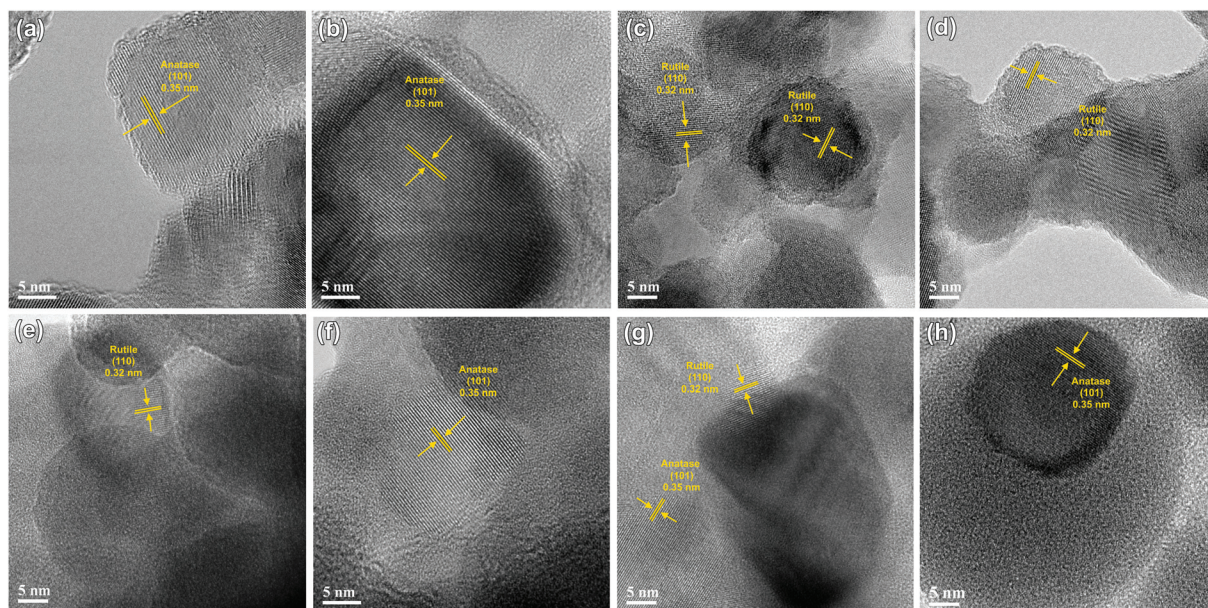
**Fig. 6** HRTEM images of TiO$_2$ powder before (a) laser ablation and after (b) 5, (c) 15, (d) 30 (e, f) 60, (g) 90, and (h) 120 minutes of laser ablation.
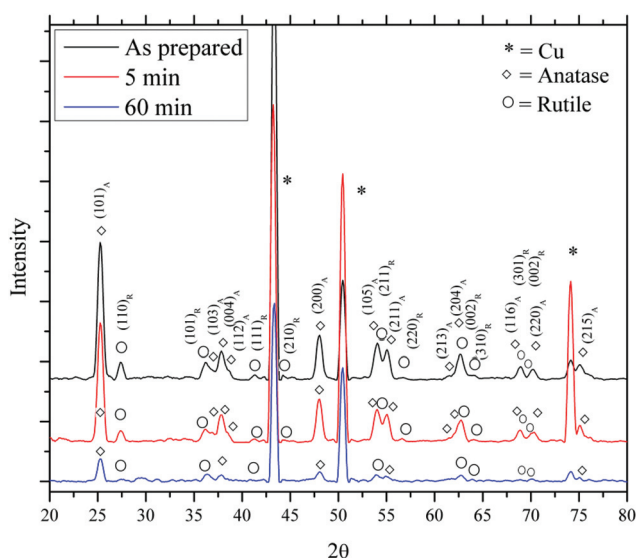


**Fig. 7** XRD analysis of the as prepared P25 dispersion and after laser treatment.

tions, (101) and (110) respectively.[65] The equation employed is given below:[65]

$$X_C = \frac{1}{1 + 1.265\left(\dfrac{I_R}{I_A}\right)} \times 100\ [\%] \qquad (1)$$

The as prepared dispersion and the ones laser treated for 5 and 60 minutes, have degree of crystallinity equal to 85.98%, 89.14% and 82.31%, respectively. It can be observed that the laser treatment did not change the level of crystallinity of the materials and the polymorphism is still present.

The energy bandgaps of the ablated dispersions were investigated. The optical bandgap of TiO$_2$ nanoparticles was calculated using Tauc's law in which the direct bandgap and indirect bandgap follow eqn (2) and (3), respectively:[56]

$$(\alpha h\nu) \propto (h\nu - E_{gap})^{1/2} \qquad (2)$$

$$(\alpha h\nu) \propto (h\nu - E_{gap})^{2} \qquad (3)$$

where $\alpha$ is the absorption coefficient, $h$ is the Planck's constant, $\nu$ is the frequency and $E_{gap}$ is the energy bandgap. As reported in the literature, anatase is an indirect bandgap semiconductor and the energy bandgap value of 3.2 eV is attributed to the $\Gamma_3 \rightarrow X_{1b}$ transition.[56] In Fig. 8(a), the normalized UV-Vis spectra of the TiO$_2$ suspensions ablated at different ablation times are shown. Based on our absorption results the plots of $(\alpha h\nu)^{1/2}$ *versus* photon energy, for indirect transitions, displayed no linear relationships. However, when the spectral data were plotted as $(\alpha h\nu)^{2}$ *versus* photon energy, a linear relationship was obtained, suggesting the occurrence of a direct band transition in an indirect bandgap semiconductor.[66] In Fig. 8(b), the Tauc plot is shown. The energy bandgap ($E_{gap}$) values of the solutions ablated at different times have been obtained by extrapolation to $\alpha = 0$, and the inset plot of the energy bandgap as a function of the laser ablation time is shown. The $E_{gap}$ values are reported in Table 1.

It was found that by increasing the ablation time, an increase in the direct energy bandgap occurred. Based on the study carried out by Nath,[56] the energy bandgap value of 3.8 eV for TiO$_2$ nanoparticles after 60 minutes of laser ablation may be attributed to either the direct interband transition of the rutile phase or to a decrease in size of the TiO$_2$ nanoparticles.[67] This result is in accordance with both the Raman and TEM results, which showed the phase transformation
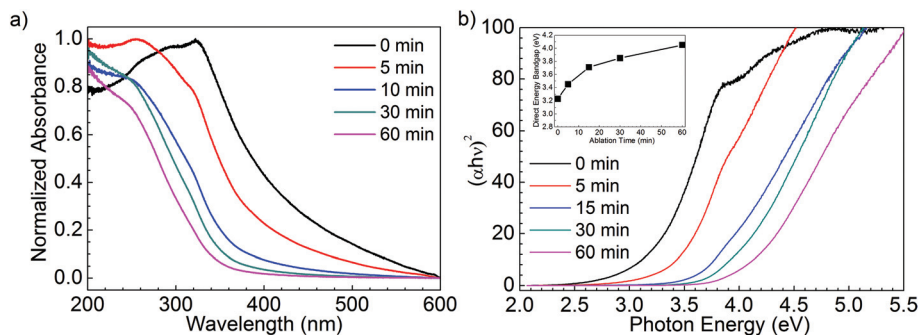
**Fig. 8** (a) UV-Vis of TiO$_2$ suspension ablated at different ablation times; (b) plot of $(\alpha h\nu)^2$ *versus* photon energy for direct transition and (inset) plot of energy bandgap values as a function of ablation time.

**Table 1** Energy gap values as a function of laser ablation time

| Laser ablation time (min) | Direct energy bandgap $(\alpha h\nu)^2$ |
| --- | --- |
| 0 | 3.2 eV |
| 5 | 3.35 eV |
| 15 | 3.7 eV |
| 30 | 3.85 eV |
| 60 | 3.9 eV |

from anatase to rutile and particle size decrease occurred after 60 minutes of laser ablation.

With proper control of the ablation time, it is possible to synthesize TiO$_2$ nanoparticles with different sizes or induce phase transformations, which lead to TiO$_2$ nanoparticles with different energy bandgap values. This opens the possibility of using PLA as a technique for bandgap engineering of TiO$_2$, such as its use in future electronic devices.[68,69]

### 3.2. Laser ablation of P25/FTO substrates

Femtosecond laser ablation was performed on P25/FTO substrates in order to compare the results from the ablation of

P25 carried out in an aqueous dispersion with the ablation of P25 deposited on a substrate. The experiments were performed by varying the laser power in order to study the phase transformation as a function of the laser power and in total 8 lines were patterned, as shown in Fig. 9. The eight lines, 1.5 cm long, were ablated at powers of 2.0, 7.0, 10, 19, 26, 38, 82, and 122 mW (Fig. 9b). The estimated fluence was calculated using the following eqn (4):

$$F = \frac{P}{1000\ \text{Hz} \times \pi r^2} \tag{4}$$

where $P$ is the power (W) and $r$ is the radius of the beam spot (cm). The beam diameter is 80 μm and the estimated fluences tested were 39.8, 139.3, 204.9, 378.0, 517.3, 756.0, 1600, and 2700 mJ cm$^{-2}$. In Fig. 9(a), lines from 3 to 8 (L3–L8) depict TiO$_2$ that is completely removed due to spallation from the femtosecond laser ablation process and only FTO glass remains on the surface, as can be seen from the surface profile (Fig. 9b). The lines patterned at powers of 2.0 and 7.0 mW (L1 and L2) showed no removal of TiO$_2$, suggesting that lower powers are preferable in order to achieve the laser patterning of the P25 on FTO/glass. The line 2 (L2) was then characterized
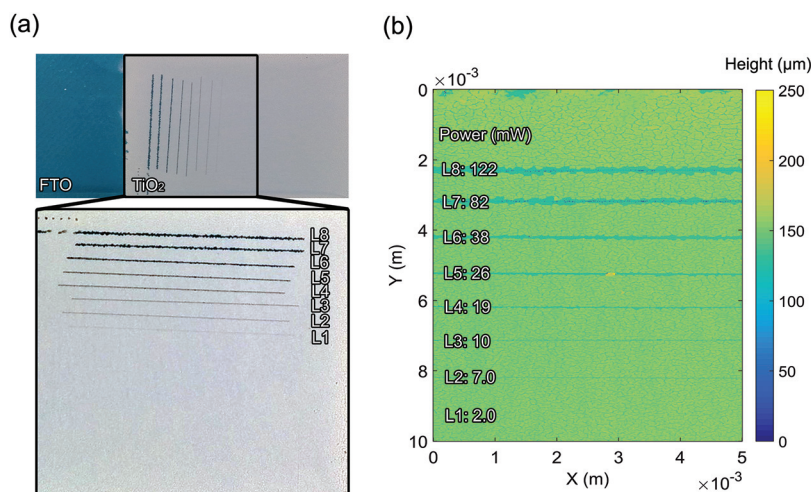


**Fig. 9** (a) Top−bottom view and (b) surface profile of P25/FTO contained femtosecond laser produced lines of varying powers.

by SEM and Raman in order to determine the morphological and crystal phase changes of $TiO_2$ after the laser interaction.

In Fig. 10, SEM images of the non-laser patterned (a, b, and c) and laser patterned (d, e, and f) regions of P25 onto FTO are shown. The electrophoretic deposition of P25 onto FTO did not form a uniform layer of P25; instead some cracks are clearly visible, as shown in Fig. 10(a). This occurs when the deposition layer is thick. A closer look at the untreated P25 film shown in Fig. 10(b) reveals the presence of a porous-like structure. Upon laser irradiation of the P25 film, a structural change occurs. Pseudo-spherical nanoparticles with sizes of 100–300 nm are formed (Fig. 10(f)), which are much larger particles than the non-treated regions (Fig. 10(c)) in which average particle size is 21 ± 5 nm. The formation of larger particles can be understood considering the underlying ablation mechanisms discussed earlier. In particular, due to the laser–

matter interaction, the local increase of temperature and pressure will take place leading to the melting and coalescence of the material and production of larger nanoparticles.[7,11,13] In order to study the effects of the laser patterning on the crystal phase of P25, Raman line mapping was performed perpendicularly from the ablated line.

The Raman line mapping is shown in Fig. 11(a), while in Fig. 11(b) the Raman spectra of the region outside the laser patterned (black spectrum) and in the middle of the laser patterned area (red spectrum) are shown. The phase transformation tends towards rutile upon laser patterning of P25 on FTO. In particular, the non-patterned P25 Raman spectrum (Fig. 11(b), black spectrum) shows the characteristic anatase peaks at 143 $cm^{-1}$, 395 $cm^{-1}$, 511 $cm^{-1}$, and 630 $cm^{-1}$.

From the Raman scan line analysis, Fig. 11(a), it can be seen that approaching the ablated center of the laser patterned
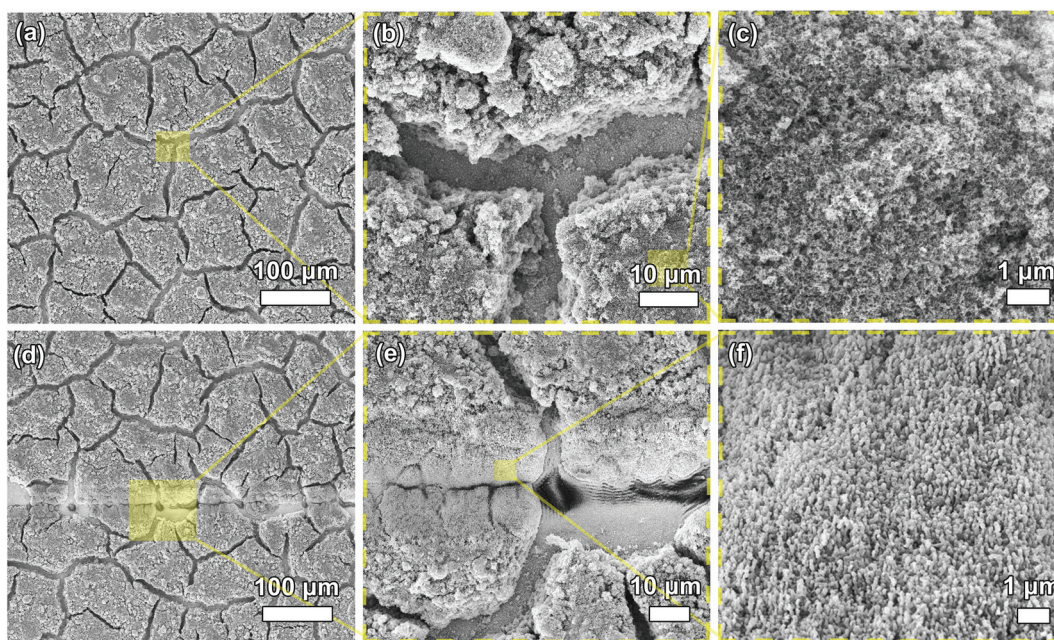


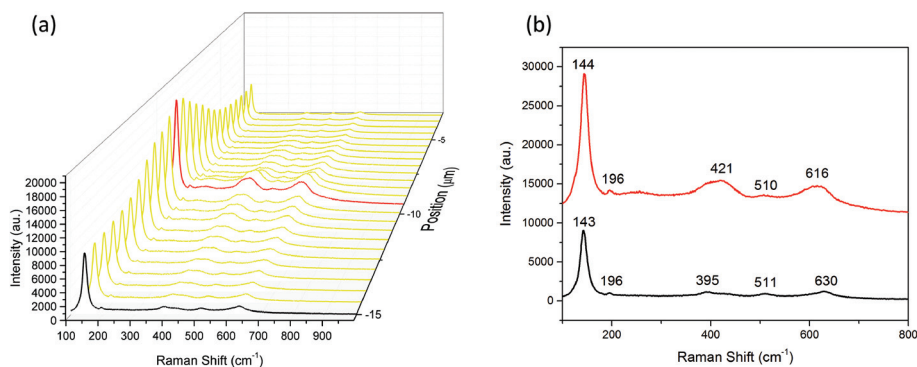Fig. 10   SEM images of (a–c) non-patterned and (d–f) laser patterned P25 on FTO.



Fig. 11   (a) Raman mapping line of laser patterned P25 on FTO; (b) Raman spectra of the area outside (black spectrum) and inside (red spectrum) the laser patterned area.

line, a redshift in the 143 cm$^{-1}$ peak occurs, and the overall spectrum shifts towards rutile-like spectrum (red). At the ablated center of the laser patterned line, broadened peaks start to appear at 421 cm$^{-1}$ and 616 cm$^{-1}$, and anatase peaks at 421 cm$^{-1}$, 395 cm$^{-1}$ and 630 cm$^{-1}$ are supressed, confirming that phase transformation of P25 to a rutile-like phase occurs along with increasing particle size in the laser affected area. It has been reported that phase transformation of TiO$_2$ crystal rutile to anatase can occur upon femtosecond laser irradiation,[7,11] however in order to achieve the transformation high temperatures and pressures are required. In our case, when the P25 substrate is irradiated in air the power employed during the laser pattering is not high enough to trigger the phase transformation to anatase. Therefore, the laser patterning induces a local increase of temperature and pressure that leads to the melting and coalescence of the material and production of larger rutile nanoparticles.[7,11,13]

The rutile phase has a higher index of refraction ($n$ = 2.9) and can scatter light more efficiently than the anatase phase ($n$ = 2.4).[70–72] This phase transformation obtained by laser patterning of TiO$_2$ films on FTO with a femtosecond laser, can open the possibility of using femtosecond laser patterned substrates in various applications such as light trapping layers in silicon solar cells, energy-harvesting devices, and dye-sensitized solar cells (DSSC).[49,50] From these results, it is clear that a femtosecond laser can be used to pattern TiO$_2$ films and by thermodynamic phase transformation, changing the crystal phase from anatase to rutile. The cross sectional profile and depth of these ablated zones can be controlled by varying the power, ablation time, scanning speed, and focus spot size.

## 4. Conclusions

In this paper we studied the effects of femtosecond laser ablation of P25 powders dispersed in water and electrophoretic deposited onto a FTO conductive substrate.

(1) The experiments indicated that when laser ablation is performed in water, depending on the laser ablation time, it is possible to induce a phase transformation of the P25 nanoparticles from anatase to rutile and then back to anatase. Although, the phase transformation from rutile to anatase is thermodynamically impossible, when the sizes of the nanoparticles decrease, a change in the phase stability occurs. In particular, for particle sizes less than 11 nm, anatase will be the most thermodynamically stable phase. When the sizes are greater than 35 nm, rutile will result in the most stable phase. At short ablation times, the particle sizes increased to slightly larger sizes. After prolonged laser exposure up to 2 hours, the particle sizes started to decrease and consequently anatase particles were formed.

(2) Together with phase transformation of the TiO$_2$ nanoparticles, an increase of the energy bandgap upon increase of the laser ablation time was found, which could be attributed to the nanoparticles size decrease induced by the fs laser ablation.

(3) Phase transformation also occurs upon laser ablation of P25 powder deposited onto FTO glass. Preliminary results show that P25 powder can be patterned and due to phase transformation to rutile, the patterned areas possess a higher refractive index leading to the possibility of using these patterned substrates for the fabrication of light trapping layers.

## References

1 G. W. Yang, *Prog. Mater. Sci.*, 2007, **52**, 648–698.
2 E. Messina, G. Compagnini, L. D'Urso, O. Puglisi, S. Bagiante and S. Scalese, *Radiat. Eff. Defects Solids*, 2010, **165**, 579–583.
3 G. Compagnini, E. Messina and O. Puglisi, *Radiat. Eff. Defects Solids*, 2008, **163**, 271–276.
4 G. Compagnini, E. Messina, O. Puglisi and V. Nicolosi, *Appl. Surf. Sci.*, 2007, **254**, 1007–1011.
5 C. N. Huang, J. S. Bow, Y. Zheng, S. Y. Chen, N. J. Ho and P. Shen, *Nanoscale Res. Lett.*, 2010, **5**, 972–985.
6 P. Liu, W. Cai, M. Fang, Z. Li, H. Zeng, J. Hu, X. Luo and W. Jing, *Nanotechnology*, 2009, **20**, 285707.
7 H. L. Ma, J. Y. Yang, Y. Dai, Y. B. Zhang, B. Lu and G. H. Ma, *Appl. Surf. Sci.*, 2007, **253**, 7497–7500.
8 F. Barreca, N. Acacia, E. Barletta, D. Spadaro, G. Currò and F. Neri, *Appl. Surf. Sci.*, 2010, **256**, 6408–6412.
9 Y. Cui, J. Sun, Z. Hu, W. Wu, N. Xu, N. Xu, Z. Ying and J. Wu, *Surf. Coat. Technol.*, 2013, **231**, 180–184.
10 A. Białous, M. Gazda, K. Grochowska, P. Atanasov, A. Dikovska, N. Nedyalkov, J. Reszczyńska, A. Zaleska-medynska and G. Śliwiński, *Thin Solid Films*, 2016, **601**, 41–44.
11 H. Ma, G. Guo, J. Yang, Y. Guo and N. Ma, *Nucl. Instrum. Methods Phys. Res., Sect. B*, 2007, **264**, 61–65.
12 M. Boutinguiza, M. Meixus, J. del Val, A. Riveiro, R. Comesaña, F. Lusquiños and J. Pou, *Phys. Procedia*, 2016, **83**, 36–45.
13 J. Medina-valtierra, C. Frausto-reyes and M. Ortiz-morales, *Mater. Lett.*, 2012, **66**, 172–175.
14 A. Hahn, *J. Laser Micro/Nanoeng.*, 2008, **3**, 73–77.
15 M. H. Tsai, S. Y. Chen and P. Shen, *J. Aerosol Sci.*, 2005, **36**, 13–25.
16 M. Boutinguiza, B. Rodriguez-gonzalez, J. Del Val, R. Comesaña, F. Lusquiños and J. Pou, *Appl. Surf. Sci.*, 2012, **258**, 9484–9486.

17 C. H. Liang, Y. Shimizu, T. Sasaki and N. Koshizaki, *J. Mater. Res.*, 2004, **19**, 1551–1557.

18 A. Fujishima, T. N. Rao and D. A. Tryk, *J. Photochem. Photobiol., C*, 2000, **1**, 1–21.

19 A. Nel, T. Xia, L. Mädler and N. Li, *Science*, 2006, **311**, 622–627.

20 B. Sha, W. Gao, X. Cui, L. Wang and F. Xu, *J. Appl. Toxicol.*, 2015, **35**, 1086–1101.

21 C. Gao, Q. Meng, K. Zhao, H. Yin, D. Wang, J. Guo, S. Zhao, L. Chang, M. He, Q. Li, H. Zhao, X. Huang, Y. Gao and Z. Tang, *Adv. Mater.*, 2016, 6485–6490.

22 J. Qi, K. Zhao, G. Li, Y. Gao, H. Zhao, R. Yu and Z. Tang, *Nanoscale*, 2014, **6**, 4072–4077.

23 K. Zhao, J. Qi, H. Yin, Z. Wang, S. Zhao, X. Ma, J. Wan, L. Chang, Y. Gao, R. Yu and Z. Tang, *J. Mater. Chem. A*, 2015, **3**, 20465–20470.

24 K. Zhao, S. Zhao, J. Qi, H. Yin, C. Gao, A. M. Khattak, Y. Wu, A. Iqbal, L. Wu, Y. Gao, R. Yu and Z. Tang, *Inorg. Chem. Front.*, 2016, **3**, 488–493.

25 S. Filice, G. Compagnini, R. Fiorenza, S. Scirè, L. D'Urso, M. E. Fragalà, P. Russo, E. Fazio and S. Scalese, *J. Colloid Interface Sci.*, 2017, **489**, 131–137.

26 M. Grätzel, *Nature*, 2001, **414**, 338–344.

27 V. Galstyan, E. Comini, G. Faglia and G. Sberveglieri, *Sensors*, 2013, **13**, 14813–14838.

28 Y. Alivov, H. Funke and P. Nagpal, *Nanotechnology*, 2015, **26**, 295203.

29 J. Wu, G. Yue, Y. Xiao, J. Lin, M. Huang, Z. Lan, Q. Tang, Y. Huang, L. Fan, S. Yin and T. Sato, *Sci. Rep.*, 2013, **3**, 1283.

30 J. van de Lagemaat, N.-G. Park and A. J. Frank, *J. Phys. Chem. B*, 2000, **104**, 2044–2052.

31 O. Carp, C. L. Huisman and A. Reller, *Prog. Solid State Chem.*, 2004, **32**, 33–177.

32 S. M. Gupta and M. Tripathi, *Chin. Sci. Bull.*, 2011, **56**, 1639–1657.

33 D. C. Hurum, A. G. Agrios, K. A. Gray, T. Rajh and M. C. Thurnauer, *J. Phys. Chem. B*, 2003, **107**, 4545–4549.

34 H. Lu, B. Zhao, R. Pan, J. Yao, J. Qiu, L. Luo and Y. Liu, *RSC Adv.*, 2014, **4**, 1128–1132.

35 V. G. Bessergenev, M. C. Mateus, A. M. B. do Rego, M. Hantusch and E. Burkel, *Appl. Catal., A*, 2015, **500**, 40–50.

36 V. N. Koparde and P. T. Cummings, *J. Phys. Chem. B*, 2005, **109**, 24280–24287.

37 V. N. Koparde and P. T. Cummings, *ACS Nano*, 2008, **2**, 1620–1624.

38 Y. Zhu, L. Zhang, C. Gao and L. Cao, *J. Mater. Sci.*, 2000, **35**, 4049–4054.

39 X. Chen and S. S. Mao, *Chem. Rev.*, 2007, **107**, 2891–2959.

40 Z. Lai, F. Peng, Y. Wang, H. Wang, H. Yu, P. Liu and H. Zhao, *J. Mater. Chem.*, 2012, **22**, 23906.

41 D. A. H. Hanaor and C. C. Sorrell, *J. Mater. Sci.*, 2011, **46**, 855–874.

42 N. H. Vu, H. V. Le, T. M. Cao, V. V. Pham, H. M. Le and D. Nguyen-manh, *J. Phys.: Condens. Matter*, 2012, **24**, 405501.

43 G. C. Vásquez, M. A. Peche-herrero, D. Maestre, A. Gianoncelli, J. Ramírez-castellanos, A. Cremades, J. M. González-calbet and J. Piqueras, *J. Phys. Chem. C*, 2015, **119**, 11965–11974.

44 S.-C. Zhu, S.-H. Xie and Z.-P. Liu, *J. Am. Chem. Soc.*, 2015, **137**, 11532–11539.

45 R. D. Shannon, *J. Appl. Phys.*, 1964, **35**, 3414–3416.

46 M. S. P. Francisco and V. R. Mastelaro, *Chem. Mater.*, 2002, **14**, 2514–2518.

47 V. Körstgens, S. Pröller, T. Buchmann, D. Moseguí González, L. Song, Y. Yao, W. Wang, J. Werhahn, G. Santoro, S. V. Roth, H. Iglev, R. Kienberger and P. Müller-Buschbaum, *Nanoscale*, 2015, **7**, 2900–2904.

48 M. A. Pugachevskii, *Tech. Phys. Lett.*, 2013, **39**, 36–38.

49 J. Qian, P. Liu, Y. Xiao, Y. Jiang, Y. Cao, X. Ai and H. Yang, *Adv. Mater.*, 2009, **21**, 3663–3667.

50 J. Du, J. Qi, D. Wang and Z. Tang, *Energy Environ. Sci.*, 2012, **5**, 6914.

51 R. Liang, M. Hatat-fraile, M. Arlos, M. Servos and Y. N. Zhou, in 14th IEEE International Conference on Nanotechnology, IEEE, 2014, pp. 975–980.

52 S. I. Alnassar, E. Akman, B. G. Oztoprak, E. Kacar, O. Gundogdu, A. Khaleel and A. Demir, *Opt. Laser Technol.*, 2013, **51**, 17–23.

53 W. F. Zhang, Y. L. He, M. S. Zhang, Z. Yin and Q. Chen, *J. Phys. D: Appl. Phys.*, 2000, **33**, 912–916.

54 J. C. Parker and R. W. Siegel, *Appl. Phys. Lett.*, 1990, **57**, 943–945.

55 C. A. Melendres, A. Narayanasamy, V. A. Maroni and R. W. Siegel, *J. Mater. Res.*, 1989, **4**, 1246–1250.

56 A. Nath, S. S. Laha and A. Khare, *Integr. Ferroelectr.*, 2010, **121**, 58–64.

57 F. Tian, J. Sun, J. Yang, P. Wu, H. L. Wang and X. W. Du, *Mater. Lett.*, 2009, **63**, 2384–2386.

58 J. Zhang, M. Li, Z. Feng, J. Chen and C. Li, *J. Phys. Chem. B*, 2006, **110**, 927–935.

59 F. Hardcastle, *J. Arkansas Acad. Sci.*, 2011, **65**, 43–48; F. D. Hardcastle, *J. Arkansas Acad. Sci.*, 2011, **65**, 43–48.

60 A. Pyatenko, H. Wang and N. Koshizaki, *J. Phys. Chem. C*, 2014, **118**, 4495–4500.

61 H. Wang, K. Kawaguchi, A. Pyatenko, X. Li, Z. Swiatkowska-warkocka, Y. Katou and N. Koshizaki, *Chemistry*, 2012, **18**, 163–169.

62 P. V. Kamat, M. Flumiani and G. V. Hartland, *J. Phys. Chem. B*, 1998, **102**, 3123–3128.

63 A. Takami, H. Kurita and S. Koda, *J. Phys. Chem. B*, 1999, **103**, 1226–1232.

64 A. Pyatenko, M. Yamaguchi and M. Suzuki, *J. Phys. Chem. C*, 2007, **111**, 7910–7917.

65 R. A. Spurr and H. Myers, *Anal. Chem.*, 1957, **29**, 760–762.

66 N. Serpone, D. Lawless and R. Khairutdinov, *J. Phys. Chem.*, 1995, **99**, 16646–16654.

67 G. Lassaletta, A. Fernandez, J. P. Espinos and A. R. Gonzalez-elipe, *J. Phys. Chem.*, 1995, **99**, 1484–1490.

68 J. Robertson, *J. Vac. Sci. Technol., B: Microelectron. Nanometer Struct.–Process., Meas., Phenom.*, 2000, **18**, 1785.

69 V. Bessergenev and H. L. Gomes, *Phys. Status Solidi C*, 2010, **7**, 949–952.

70 D. Eder, I. A. Kinloch and A. H. Windle, *Chem. Commun.*, 2006, **30**, 1448–1450.

71 X. Zhang, L. Chen, H. Pan, Z. Bao and X. Zhou, *Thin Solid Films*, 2014, **573**, 107–111.

72 H. Zhang, X. Liu, Y. Li, Q. Sun, Y. Wang, B. J. Wood, P. Liu, D. Yang and H. Zhao, *J. Mater. Chem.*, 2012, **22**, 2465–2472.